Acta Polytechnica **66**(2):185–195, 2026
https://doi.org/10.14311/AP.2026.66.0185

Published by the Czech Technical University in Prague

RHEOLOGICAL BEHAVIOUR AND REACTION KINETICS IN ALKALI-ACTIVATED SLAG-METAKAOLIN BLENDS WITH LIMESTONE SLUDGE

Dana Kubátová*, Eliška Křivánková, Martin Nguyen, Michaela Krejčí Kotlánová, Martin Boháč

Research Institute for Building Materials, Hněvkovského 65, 617 00 Brno, Czech Republic

* corresponding author: kubatova@vush.cz

Abstract. This study focuses on the influence of raw limestone materials on the fresh-state properties and early hydration behaviour of alkali-activated systems composed of blast furnace slag and metakaolin. Three types of limestone powders were examined in relation to their rheological impact, structural rebuilding (via oscillatory strain-amplitude sweeps and 3iTT tests), calorimetric behaviour, and thermal stability (TG/DTG). The results show that, at early stages, limestone primarily acts as an inert filler, but its particle morphology and impurity content significantly affect the system's rheology and reaction kinetics. Limestone powder with high calcite content slightly accelerates structural regeneration and improves dispersion, while limestone powders containing clay minerals increase plasticity and stiffness due to water retention and enhanced interparticle interactions. Such clay-bearing powders can, however, also slow structural rebuilding and reduce flowability under shear. Calorimetry and thermal analysis confirmed that limestone powder addition, especially in low-calcium systems, promoted the formation of hybrid gels (C-(A)-S-H and N-A-S-H). Clay-related alumina also significantly affected both the early-age rheology and the reaction kinetics.

Keywords: Limestone sludge, limestone powder, alkali activation, rheology, early-stage reaction kinetics.

1. Introduction

Alkali-activated materials (AAMs) are a sustainable alternative to Portland cement due to their lower CO_2 emissions, reduced energy use, and superior mechanical properties. They are produced by activating aluminosilicate-rich materials, such as fly ash, slag, or metakaolin with alkaline solutions. The addition of various types of cementitious materials has gained increasing attention in recent years due to their accessibility and diverse functionalities, offering enhanced properties depending on the material selected.

Recent studies have explored the addition of limestone powder (LS) and limestone sludge in order to enhance the performance of AAM. Previous studies have extensively examined the effects of limestone on the fresh and hardened properties of various types of alkali-activated binders. Different types of limestone powders, with varying chemical compositions and CaO content, have been tested in systems, such as slag-based alkali-activated materials [1–3], metakaolin-based systems [4–6], and fly ash-based matrices. These studies have provided valuable insights into the influence of limestone on reaction kinetics, workability, mechanical properties, and other critical aspects of the alkali-activation process.

In general, incorporating LS into alkali-activated systems has been shown to improve workability. As the content of LS increases, the workability of the mixture also increases, which can be attributed to the finer particles of limestone that enhance particle packing and reduce friction between particles. This results in a more fluid mix that is easier to handle during processing. Moreover, higher amounts of LS are correlated with improved flowability, and the increased presence of LS can accelerate the hydration and activation processes, thereby enhancing early-age strength development of the binder. However, it is crucial to note that the optimum ratio of LS varies depending on the specific precursor material used. If the amount of LS exceeds a certain threshold, it may negatively impact the overall strength and durability of the resulting alkali-activated binder due to the dilution effect or the potential for unwanted chemical reactions between the components [1, 7]. Similar nucleation/filler versus dilution trends have been reported for both slag-based and metakaolin-based alkali-activated binders, although the magnitude and even the direction of the effect may depend on the activator chemistry, limestone fineness, and mineralogical impurities [8, 9]. It should be mentioned that most of the studies used limestone powders with relatively low Al_2O_3 content not exceeding 3 %. The influence of Al_2O_3, which is not a primary component in limestone and whose sources may include clay minerals, feldspars, or micas, has not been evaluated in detail in these studies.

The evaluation of workability in AAMs is typically performed using traditional mini slump tests, which help assess the ease with which the material can be

	SiO_2	Al_2O_3	CaO	Na_2O	K_2O	MgO	Fe_2O_3	SO_3	TiO_2	LOI
LS1	0.75	0.29	53.26	0.07	0.03	0.29	0.23	0.01	0.01	43.49
LS2	19.6	3.11	41.50	0.09	0.46	0.26	1.40	0.01	0.24	33.25
LS3	20.32	9.04	34.37	0.18	1.2	0.67	3.16	0.02	0.46	30.23
BSF	39.90	8.25	36.17	0.65	0.52	8.32	0.49	0.94	0.31	1.90
MK	52.21	42.94	0.20	0	0.78	0.28	0.92	1.56	0.05	2.10

Table 1. Chemical composition of raw materials.

placed and shaped. Rheological properties are also a key consideration, and advanced rheological equipment such as rotational rheometers are often employed to obtain more precise data on the flow behaviour of these materials under different conditions. The rheological behaviour of AAMs is commonly modelled using two mathematical models: the Bingham model and the Herschel-Bulkley model. Both models describe the flow characteristics of materials with yield stress and viscosity-related parameters, which are critical for applications such as grouting, casting, and 3D printing [10–12]. However, alkali-activated pastes can exhibit rapid, time-dependent structural build-up after mixing and the fitted parameters may be strongly affected by shear history and the specific steady-shear protocol; therefore, obtaining robust Bingham/Herschel-Bulkley parameters would require dedicated flow-curve testing beyond the scope of this work [13–15]. This choice is consistent with recent SAOS-based studies on structural build-up, where strain amplitude sweeps are used to capture the evolving LVR and provide additional information on structural breakdown at early ages [11, 13, 16]. Accordingly, this study focuses on early-age structuration and thixotropy assessed by oscillatory amplitude sweeps and 3iTT.

The primary aim of this study is to gain a deeper understanding of the influence of limestone sludge on the rheology and early-stage reaction kinetics of alkali-activated metakaolin-blast furnace slag mixtures. This work complements previous research [17] focused primarily on the long-term properties of alkali-activated materials (AAMs).

As the early-age workability and kinetics strongly influence the processing and application, the evolution of the system was monitored from the end of mixing for up to 24 hours. The upper limit of the linear viscoelastic region (LVR) and the crossover point of the viscoelastic moduli G'/G'' were determined by an oscillatory strain-amplitude sweep [13], which identifies the deformation level at which the material departs from the linear regime and starts to yield/flow. Data from the three-interval thixotropy test (3iTT) were used to evaluate the restructuring of the sample over time after the application of shear stress [18]. The effect of limestone dust on reaction kinetics was assessed using isothermal calorimetry.

	D_{10}	D_{50}	D_{90}	Mean diameter
LS1	0.78	5.30	27.41	9.82
LS2	1.42	9.27	25.15	11.72
LS3	2.39	18.19	45.78	21.79
BSF	1.71	10.44	26.03	12.45
MK	1.62	6.09	12.38	6.66

Table 2. Particle size distribution of raw materials [µm].

2. Materials and methods

2.1. Materials characterisation

The raw materials used in this study included metakaolin (MK), blast furnace slag (BFS), and three types of raw limestone meal (LS). The MK Mefisto L05 was provided by České lupkové závody, a.s. (Czech Republic), while the finely ground BFS was sourced from Třinec (Czech Republic). The limestone materials were produced from Vitošov limestone (Czech Republic). LS1 was prepared by grinding the limestone rock, while LS2 and LS3 were waste materials generated during limestone mining and washing; both originated from the same process, but were collected in different batches, which may explain their compositional variability.

During processing, the sludge is mixed with washing water and directed to a sludge pond, where it settles. This settled sludge is currently not utilised and its accumulation in the landfill continues to grow. Prior to testing, the samples were dried at 60 °C and subsequently ground.

The chemical composition was analysed by X-ray fluorescence and is shown in Table 1, while the characteristic particle sizes (D_{10}, D_{50}, and D_{90}) are listed in Table 2. The detailed particle size distributions are shown in Figure 1.

X-ray diffraction (QXRD) was employed to determine the mineralogical composition of the raw materials. In addition to the amorphous phase, the slag contained crystalline phases, such as calcite ($CaCO_3$), gypsum ($CaSO_4{\cdot}2H_2O$), quartz (SiO_2), wollastonite ($CaSiO_3$), anorthite ($CaAl_2Si_2O_8$), gehlenite ($Ca_2Al(AlSi)O_7$), merwinite ($Ca_3Mg(SiO_4)_2$), and sanidine ($K(AlSi_3O_8)$). Metakaolin exhibited an amorphous phase along with kaolinite ($Al_2Si_2O_5(OH)_4$), quartz (SiO_2), il-

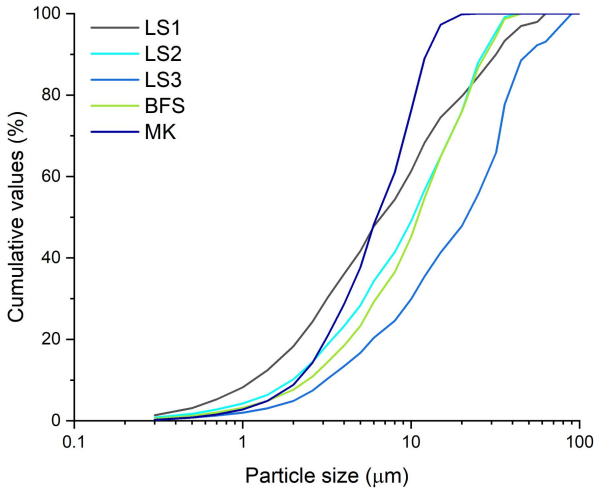

FIGURE 1. Particle size distribution of raw materials.

lite ($(K, H_3O)(Al, Mg, Fe)_2(Si, Al)_4O_{10}(OH)_2 \cdot H_2O$), anatase ($TiO_2$), and mullite ($Al_6Si_2O_{13}$). The primary phase in LS1 and LS2 was calcite ($CaCO_3$), with minor amounts of muscovite ($KAl_2(AlSi_3O_{10})(OH)_2$), illite, and quartz ($SiO_2$). LS3 additionally contained rutile (TiO_2), orthoclase ($KAlSi_3O_8$), albite ($NaAlSi_3O_8$), anorthite ($CaAl_2Si_2O_8$), and kaolinite ($Al_2Si_2O_5(OH)_4$). Thermogravimetric and differential thermal analysis (TG/DTG) was used to quantify the $CaCO_3$ content in the limestone samples and to support the characterisation of the AAM samples. The results showed that LS1 contained 97.6 wt. % of $CaCO_3$, LS2 contained 71.65 wt. % of $CaCO_3$, and LS3 contained 63.4 wt. % of $CaCO_3$.

2.2. Sample preparation

MK, BFS, and LS were weighed in various proportions, with the LS content ranging from 0 to 30 wt. %. Two series of samples were prepared. For the SM1 series, the samples were slag-rich (BFS = 54.6–78 wt. % of slag), whereas in the SM2 series, the mixtures were metakaolin-rich (BFS = 31.1–44.4 wt. % of slag). The mixture compositions are summarised in Table 3. The sodium silicate solution (22.2 wt. % of SiO_2 and 12.4 wt. % of Na_2O) was used as the alkaline activator. After dry homogenisation, the activator was added at a constant liquid-to-binder ratio, and the paste was mixed for 2 minutes.

2.3. Testing methods

The composition of raw materials and hardened samples after 7 days was analysed using X-ray powder diffraction. This analysis was performed using a Bruker D8 Advance apparatus equipped with a Cu anode ($\lambda K\alpha = 1.54184$ Å) and variable divergence slits, in Θ-Θ Bragg-Brentano reflection geometry setup. The particle size distribution (PSD) of raw materials was measured using a CILAS 920L laser particle size analyser with a measurement range of 0.3–400 µm.

	BFS	MK	LS
SM1	78.0	22.0	0
SM1 10LS	70.2	19.8	10
SM1 30LS	54.6	15.4	30
SM2	44.4	55.6	0
SM2 10LS	40.0	50.0	10
SM2 30LS	31.1	38.9	30

TABLE 3. Composition of samples (LS = LS1, LS2 or LS3).

The rheological parameters were monitored using a DHR-1 rotational rheometer (TA Instruments) equipped with a coaxial cylinder measuring geometry, a four-blade rotor, and a cup with vertical ribbing. Measurements were performed at 25 °C. The total mixing time was 2 minutes, after which the paste was immediately transferred into the measuring cup. First, the sample was pre-sheared at 100 s^{-1} for 60 seconds, followed by a 60-second resting equilibration, so the actual measurement started 5 minutes after the end of mixing. An oscillatory amplitude sweep was conducted to determine the upper limit of the linear viscoelastic region (LVR) and the crossover point ($G' = G''$), indicating the onset of yielding/flow; the strain amplitude was logarithmically increased from 5×10^{-4} to 500 % at an angular frequency of $\omega = 10$ rad s^{-1} [19]. The maximum value of G' was considered as the LVR limit [13]. Thixotropy, i.e. time-dependent structural rebuilding after shear, was evaluated from the evolution of viscosity using the three-interval thixotropy test (3iTT) [18, 20]. The 3iTT protocol consisted of three intervals:

(1.) A low shear rate of 0.01 s^{-1} for 5 min to represent a resting state;

(2.) a high shear rate of 100 s^{-1} for 30 s to break down the structure;

(3.) a return to 0.01 s^{-1} to monitor structural regeneration.

The rate of rebuilding was quantified from the initial slope of the "plastic viscosity recovery" in the third interval, in accordance with DIN/TR 91143-2:

$$\frac{\Delta\eta}{\Delta t} = \frac{\eta_3 - \eta_2}{60} \quad [\text{Pa}], \tag{1}$$

where η_2 is the shear viscosity at the end of the high-shear interval (second interval), and η_3 is the shear viscosity achieved 60 s after the start of the third interval. Time was expressed in seconds to match the viscosity-time units used in the calculation.

The fresh pastes were analysed using a TAM Air 8-channel isothermal calorimeter (TA Instruments) at 25 °C. The pastes were prepared by mixing them with a sodium silicate solution ($\frac{w}{s} = 0.8$) ex situ. Ampoules containing 4 g of paste were placed into the calorimeter three minutes after the mixing. Heat

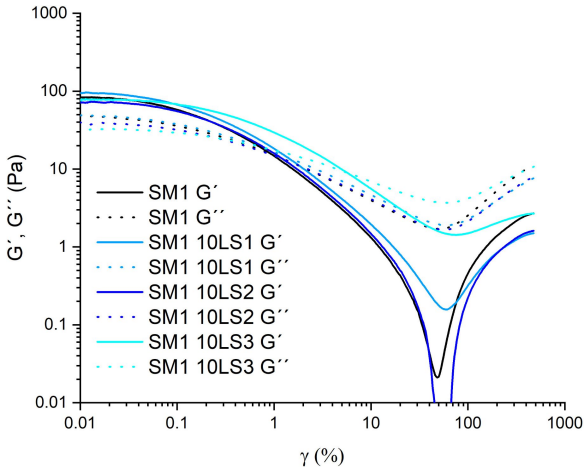

(a). 10 wt. % of LS.

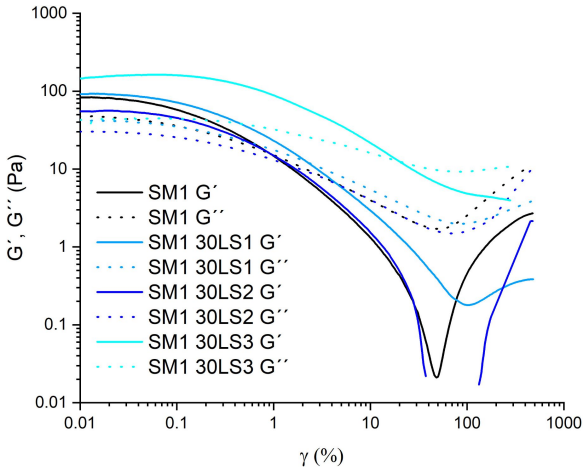

(b). 30 wt. % of LS.

Figure 2. Strain amplitude sweeps of samples SM1.

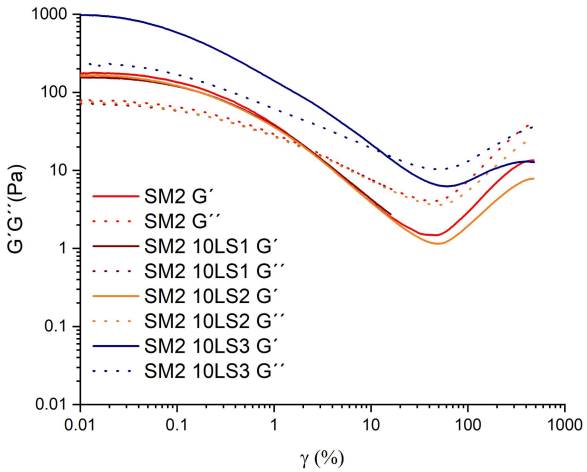

(a). 10 wt. % of LS.

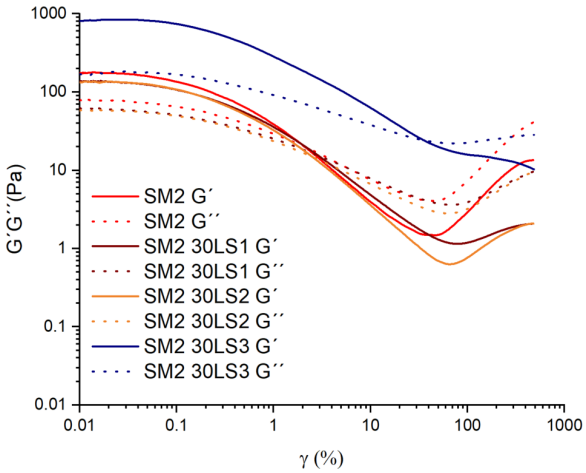

(b). 30 wt. % of LS.

Figure 3. Strain amplitude sweeps of samples SM2.

flow and cumulative heat release were measured for 24 hours.

Thermogravimetric and differential thermal analyses (TG/DTG) were conducted on LS samples (250.0±0.1 mg) and hardened samples using a STA 449 F3 Perseus (Netzsch) under a dynamic synthetic air atmosphere. The temperature range was 35–1 100 °C with a heating rate of 10 °C per minute.

3. Results and discussion

3.1. Rheology

3.1.1. Amplitude test

As can be seen from Figures 2 and 3, at low strains, all mixtures behave as viscoelastic solids because G' predominates over G''. After the crossover point ($G' = G''$; see Table 4), the response becomes more liquid-like, which is typical of fine-particle dispersions such as fresh alkali-activated pastes.

When comparing SM1 and SM2, the influence of the precursor composition is apparent: with an increasing slag fraction (SM1) at the expense of metakaolin quantity, the overall moduli decrease and the crossover tend to occur at a lower strain, indicating earlier yielding. At this early stage, the rheological response is governed primarily by reversible physical interactions rather than by chemical bonding.

In contrast, metakaolin-rich mixtures (SM2) exhibited higher moduli and a more solid-like response, which is consistent with the larger specific surface area of metakaolin and its layered structure that enhances liquid retention [21]. Conversely, the presence of smooth, glassy slag particles tends to enhance flowability, particularly in sodium silicate (waterglass)-activated systems, consistent with the shift of the crossover towards lower strains in SM1. In addition, G'' was closer to G' for the SM1 than in the case of SM2, indicating a larger viscous contribution associated with the higher liquid-phase mobility in the slag-rich mixtures.

Figures 2 and 3 illustrate the effect of limestone replacement. For LS1, only minor changes were observed in both series. Based on the slope in the pre-yield region, plasticity increased slightly with increasing LS1

SM1	**0LS**	**10LS1**	**30LS1**	**10LS2**	**30LS2**	**10LS3**	**30LS3**
LVR limit [%]	1.32×10^{-2}	1.10×10^{-2}	7.56×10^{-3}	1.28×10^{-2}	1.20×10^{-2}	1.10×10^{-2}	6.48×10^{-2}
G', G'' crossover [%]	0.92	1.36	2.24	1.22	1.50	5.70	19.99

SM2	**0LS**	**10LS1**	**30LS1**	**10LS2**	**30LS2**	**10LS3**	**30LS3**
LVR limit [%]	1.44×10^{-2}	9.32×10^{-3}	6.13×10^{-3}	1.52×10^{-2}	1.87×10^{-2}	9.21×10^{-3}	2.50×10^{-2}
G', G'' crossover [%]	2.08	2.39	2.90	2.30	2.52	13.28	35.50

TABLE 4. Limit values of LVR and the crossover of the samples' shear moduli.

content, which may be attributed to the fine particle fraction and a filler/packing effect [5]. This trend was weaker for the slag-rich series (SM1, Figure 2) than for the metakaolin-rich series (SM2, Figure 3). At this early age, chemical contribution of Ca^{2+} ions released by limestone dissolution is unlikely because calcite dissolution is relatively slow. The crossover strain increased only slightly with increasing LS content, indicating that a greater deformation is required to break the structure. Similarly, the LS2 replacement in SM2 exhibited only a minor effect in the oscillatory mode (Figure 3), and the crossover trend remained consistent.

In contrast, LS2 affected the moduli of SM1 (Figure 2) more markedly than those of SM2 (Figure 3), mainly by shifting G' and G'' to lower values, although this effect is largely confined to the LVR region. However, once the flow transition point was reached ($G' = G''$), the post-yield response became similar across all mixtures over a certain strain range, regardless of the limestone sludge replacement amount (partial replacement of the curves), and at higher strains, the response was increasingly influenced by experimental artefacts related to sample/instrument inertia.

The most pronounced effect was observed for LS3, for which both G' and G'' shift to higher values (Figures 2 and 3). This is consistent with the higher content of clay-related impurities in LS3, which increases water demand and strengthens interparticle interactions. Clay minerals, such as kaolinite or illite, possess a high specific surface area and a layered structure that can trap and retain water, thereby increasing stiffness and apparent solid-like behaviour [21]. Across the whole dataset, G'' was smaller than G', but this difference is more pronounced for LS3, indicating a firmer structure with a dominant elastic contribution. Stronger interparticle interactions are also reflected by the crossover occurring at substantially higher strain. Moreover, the less steep post-yield trend suggests increased plasticity, attributable primarily to higher internal friction within the suspension.

It should be noted that, for low-modulus (very fluid) pastes, the LVR limit values (Table 4) may be affected by instability in the moduli at very low strains; therefore, the trend is generally clearer for crossover strains than for the LVR limits.

3.1.2. Restructuration based on plastic viscosity and 3-step procedure (3ITT)

Figures 4 and 5 display the time-dependent plastic viscosity of the examined samples. For clarity, Figure 4 presents the slag-rich series SM1 (higher BFS/MK ratio), whereas Figure 5 presents the metakaolin-rich series SM2 (lower BFS/MK ratio).

When comparing the two precursor series, the effect of precursor composition becomes clear: as the amount of slag increases, fluidity is enhanced. This trend is consistent with waterglass-activated binders, where increasing the slag fraction generally improves early-age flow but can also accelerate time-dependent structural build-up due to a rapid precipitation of early reaction products. Conversely, metakaolin-rich pastes may exhibit a more viscosity-dominated response controlled by the alkaline silicate solution [22, 23]. Accordingly, SM1 exhibited lower plastic viscosity during the high-shear interval compared to SM2.

As can be seen from the related slopes in Table 5, structural regeneration after the high-shear step decreased and mixtures with higher slag content were generally more prone to sagging. This observation aligns with the amplitude sweep measurements and is also consistent with previously reported sensitivity of fresh-state rheology to the slag/metakaolin ratio in alkali-activated binders [11, 13].

Considering the limestone replacement level, a 30 wt. % limestone replacement provides better flowability within the high-shear rate interval. This suggests that fluidity during fast mixing is influenced more by the segregation of the liquid phase, particle shape, and morphology than by the fine fraction or clay impurities, although their contribution remains significant. Within each series, lower viscosities were observed for SM1 samples, while SM2 samples, which contain less slag, exhibited higher viscosities. Across both series, the limestone additions showed consistent qualitative trends: LS3 significantly thickened the samples, promoting stronger structural build-up, while LS1 slightly facilitated structural re-

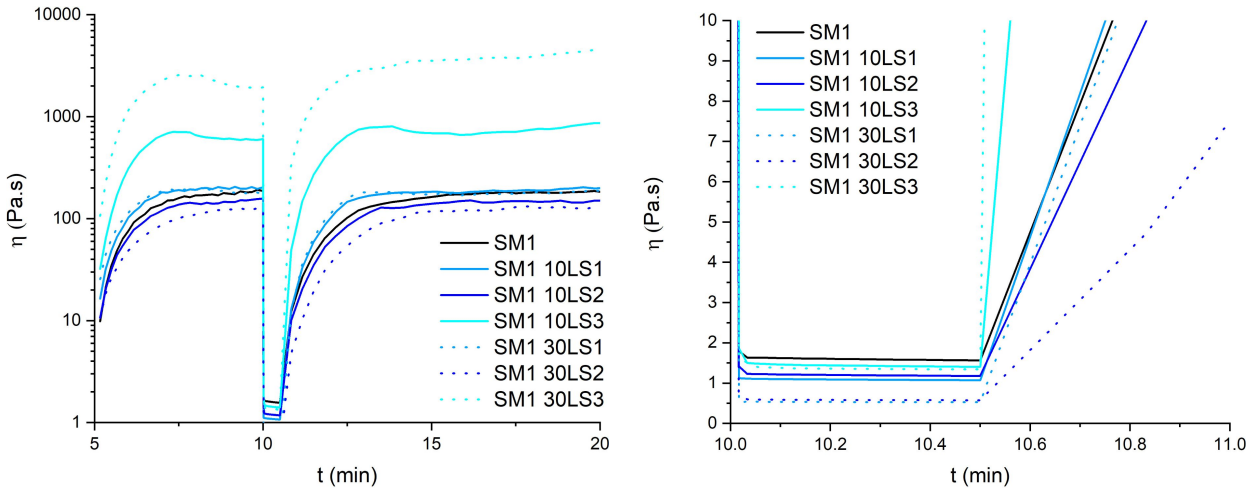

(a). 3iTT test.

(b). Detailed view of plastic viscosity at the high shear rate step.

Figure 4. Time-dependent viscosity curves for SM1 sample series.

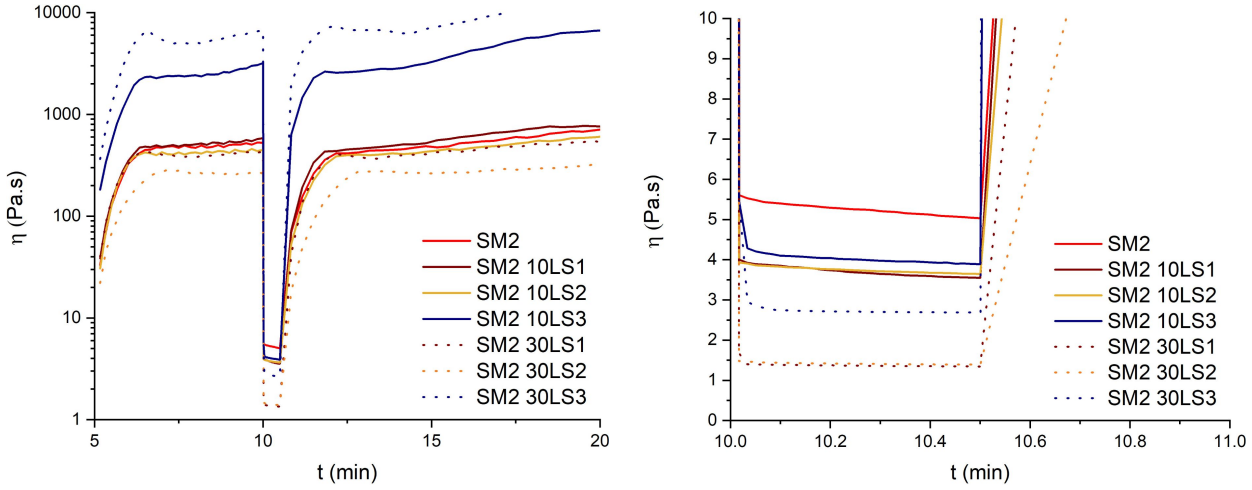

(a). 3iTT test.

(b). Detailed view of plastic viscosity at the high shear rate step.

Figure 5. Time-dependent viscosity curves for SM2 sample series.

Sample	η_2 **[Pa s]**	η_3 **[Pa s]**	$\Delta\eta$ **[Pa s]**	**Slope [Pa]**
SM1	1.56	44.41	42.8	0.7
SM1 10LS1	1.07	58.88	57.8	1.0
SM1 10LS2	1.18	34.92	33.7	0.6
SM1 10LS3	1.40	269.03	267.6	4.5
SM1 30LS1	0.53	64.94	64.4	1.1
SM1 30LS2	0.58	19.30	18.7	0.3
SM1 30LS3	1.34	1 331.76	1 330.4	22.2
SM2	5.03	262.19	257.2	4.3
SM2 10LS1	3.54	336.74	333.2	5.6
SM2 10LS2	3.65	225.07	221.4	3.7
SM2 10LS3	3.89	2 281.46	2 277.6	38.0
SM2 30LS1	1.35	247.14	245.8	4.1
SM2 30LS2	1.40	91.82	90.4	1.5
SM2 30LS3	2.68	5 719.82	5 717.1	95.3

Table 5. Measured parameters and related slopes describing the structure regeneration rate based on Equation (1).

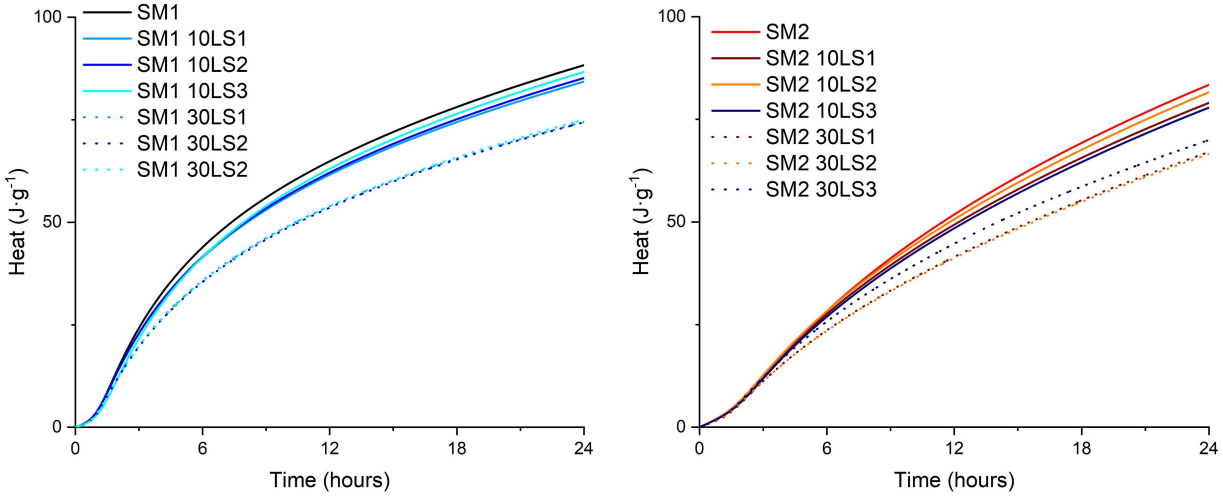

(A). SM1. (B). SM2.

FIGURE 6. Cumulative heat release of pastes with limestone powder.

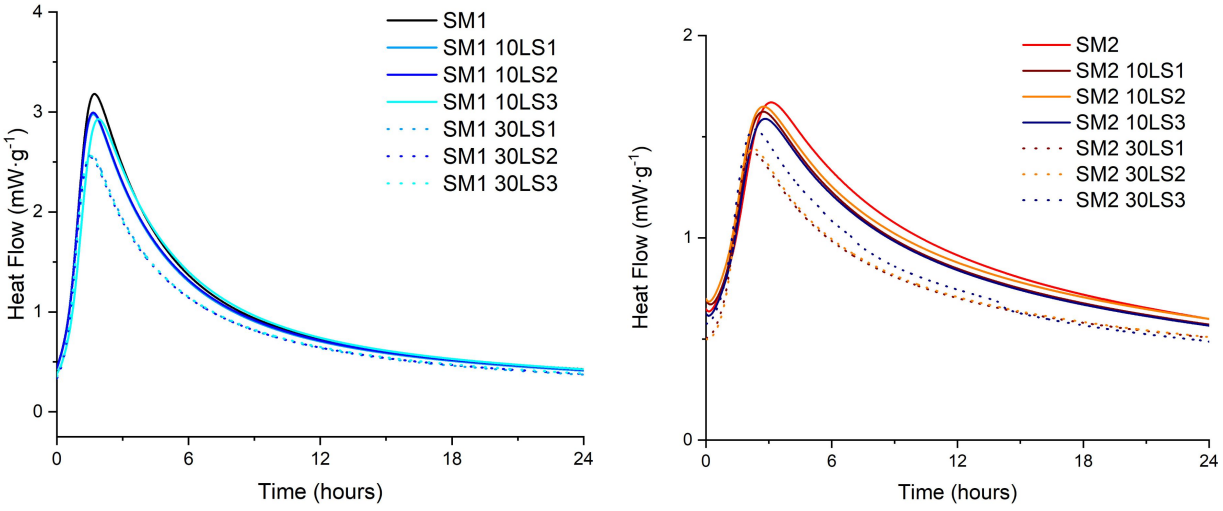

(A). SM1. (B). SM2.

FIGURE 7. Normalised heat flow of pastes with limestone powder.

generation, suppressing the self-spreading behaviour only marginally. These trends are more clearly quantified in Table 5. The replacement level enhances the observed effects [5].

Interestingly, a different effect can be observed for LS2. According to Table 5, the LS2 slowed down the structural regeneration (lower slope), which means that the sagging tendency increased compared to the reference pastes SM1 or SM2. This may be related to the different mineralogical composition of LS2.

3.2. ISOTHERMAL CALORIMETRY

Isothermal calorimetry complemented the rheological measurements and was used to investigate the reaction kinetics over a 24 h period. The normalised heat flow and cumulative heat release of blends containing blast furnace slag, metakaolin, and various limestone powders, activated with a sodium silicate solution (waterglass), during the first 24 hours are presented in Figures 6 and 7. Figure 6 illustrates the evolution of cumulative heat released during the first 24 h of hydration. The total cumulative heat after 24 hours reached 88 J g^{-1} for the reference mixture SM1, whereas for SM2, it slightly decreased to 83 J g^{-1}. However, as the limestone powder content in the mixture increases, the final cumulative heat after 24 hours decreases. This trend reflects the lower reactivity of limestone compared to slag and metakaolin, leading to a reduction in the amount of reaction products formed in the early hydration stages [24]. An exception was observed for SM2 30LS3, which exhibited a higher cumulative heat release. This behaviour is likely related to the higher clay/fine impurity fraction in LS3: fine clay particles, such as kaolinite or illite, contribute to the formation of additional aluminosilicate gel phases and elevate the early heat evolution [25].

The heat flow curves display three characteristic reaction phases: initial dissolution, induction period, and dissolution/precipitation [26]. The initial phase, associated with the wetting and partial dissolution

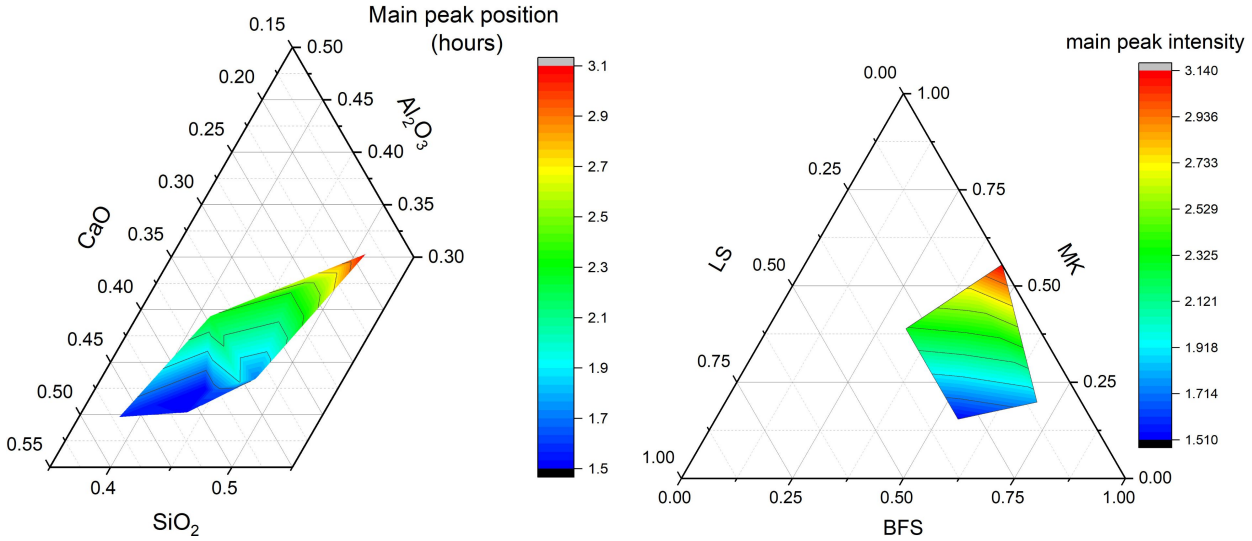

(A). Effect of theoretical chemical composition on the position of the main heat release peak.

(B). Effect of raw material composition on the main peak intensity.

Figure 8. Effect of composition on the position and intensity of the main heat release peak.

of raw materials, typically occurs within a few minutes after mixing. This phase is primarily physical in nature, although some early chemical reactions may also take place. The first 40 minutes, during which the most intense calorimetric peaks occur, are not included in the graphs for clarity. Following the induction period, a second exothermic peak appears, which corresponds to the extensive formation of reaction products from the dissolved precursors.

The intensity of the main peak for mixtures with higher slag content (SM1) ranged from 2.5 to 3.25 mW g^{-1}, while for SM2 mixtures, the heat flow was lower, ranging from 1.4 to 1.6 mW g^{-1}. Figure 8b displays the effect of raw material composition on the main peak intensity. As the CaO content increased and the Al_2O_3 content decreased, the peak intensity diminished (see Figure 8a). A higher limestone content reduced the availability of Si, Al, and Ca elements in the solution, resulting in less intense dissolution and reaction processes. These findings are consistent with previous studies. Dai [11] reported that for ternary mixtures of slag, fly ash, and limestone, increasing the LS content shifts the main peak to earlier times. The highest heat release was observed for mixtures containing 40 % LS and 10 % fly ash (FA). The acceleration of hydration is attributed to LS providing additional nucleation sites, thereby promoting the precipitation and growth of reaction products [3, 7]. In contrast, in the present metakaolin-slag system, both precursors were already highly reactive at early ages, therefore, the net effect of limestone additions reflected the balance between the nucleation/filler effect and dilution and/or impurity-related retardation [7, 27]. Accordingly, while the main peak intensity generally decreases with increasing limestone replacement, a slight shift of the main peak to later times can be observed for SM1 with LS3, which may be associated with the higher clay/fine impurity fraction of this sludge.

3.3. Thermogravimetric analysis

The X-ray diffraction analyses did not confirm the formation of new crystalline phases, which may suggest that the reaction products were predominantly amorphous or below the detection limit of the method. In this study, the TG/DTG thermal analysis was used to characterise the reaction products. Samples removed from the isothermal calorimeter after 24 h were used for the analysis. Figure 9 shows the TG/DTG curves. The total mass loss was 11.2 % for the slag-rich reference (SM1) and 13.3 % for the metakaolin-rich reference (SM2). For SM1, the characteristic peak with a maximum at 132 °C corresponds to the dehydration of N-A-S-H and C-A-S-H gels. For SM2, this peak is more pronounced, indicating a higher amount of bound water in the early-age reaction products. Another, more significant mass loss was recorded within the temperature ranges of 660–720 °C and 770–815 °C. These peaks correspond to $CaCO_3$ originating from the slag and to $CaCO_3$ formed by carbonation. For the sample with a lower slag content (SM2), only one peak is present between 660 and 720 °C [3].

The total mass loss of mixtures containing limestone (LS) increased proportionally with the amount of limestone raw material. In the temperature range of 50–1 000 °C, the mass loss ranged between 13 and 18 %. As the amount of limestone in the mixture increased, a more pronounced peak appeared in the temperature range of 720–815 °C, corresponding to the decomposition of calcite. The intensity of the first peak corresponding to the loss of free water and the dehydroxylation of C-(A)-S-H and N-A-S-H gels [28] and clay minerals, varies depending on both the content and the purity of the limestone in the mixture.

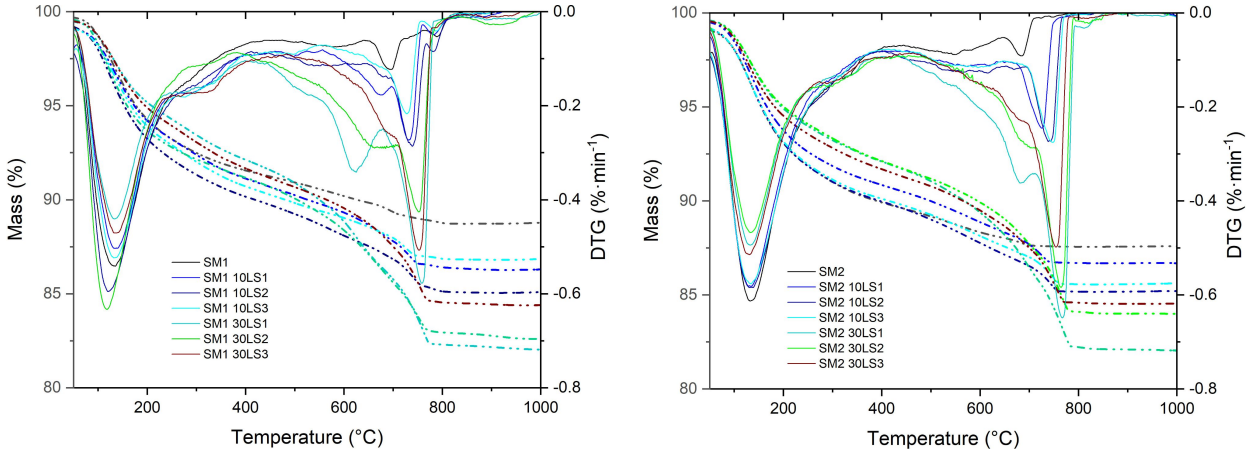

(A). SM1. (B). SM2.

FIGURE 9. Results of TG/DTG analysis.

A correlation has been observed between the chemical composition of the mixtures and mass loss in the 50–250 °C range, which decreased with increasing CaO content, suggesting that reactive CaO supplied by slag governs early gel formation and associated bound water. The dissolution rate of slag is relatively high, while limestone dissolves slowly. In mixtures with excess metakaolin (SM2 series), the correlation with the chemical composition is clearer, which may be related to the fact that limestone slightly promotes the dissolution of metakaolin and the nucleation effect. These findings are in agreement with previous studies that demonstrated the reactive potential of LS in low-calcium systems [3, 29].

4. Conclusion

This study investigated the influence of mix design – specifically the proportions of ground granulated blast furnace slag (BFS), metakaolin, and three limestone additives – on the fresh-state rheology, early-age reaction kinetics, and development of reaction products in alkali-activated systems. A comprehensive experimental programme combining rheological testing (amplitude sweeps and 3iTT), isothermal calorimetry, and thermogravimetric analysis (TG/DTG) was employed to establish a relationship between the physical response of fresh pastes and their evolving chemistry. The results highlight the coupled effect of the slag-to-metakaolin ratio and limestone characteristics, including the role of clay-related impurities in limestone residues.

The fresh-state behaviour and early hydration kinetics of alkali-activated systems were strongly governed by the slag-to-metakaolin ratio and the type of limestone powder. Rheological measurements revealed that increased slag content enhances flowability and accelerates early reactions, but simultaneously reduces structural regeneration, increasing the risk of paste sagging. In contrast, the metakaolin-rich mixtures exhibited higher stiffness and a more elastic response, consistent with stronger particle-liquid interactions and higher water retention. At very early ages, the rheological response was dominated primarily by reversible physical interactions, whereas chemical binding became increasingly important as reaction products developed.

Isothermal calorimetry and TG/DTG confirmed that changes in the theoretical chemical composition of the mixtures significantly affected reaction kinetic and the properties of formed reaction products. This effect is particularly evident in systems with a lower calcium content, where the addition of limestone promotes the formation of hybrid gel phases, such as C-(A)-S-H and N-A-S-H, which contribute to higher strength and matrix density. Alumina associated with clay impurities contributed to measurable changes in both early-age rheology and reaction kinetics.

The influence of each individual limestone powder was mixture-dependent and cannot be generalised solely by the replacement level. The observed behaviour results from the combined effects of mineralogy, particle size distribution, and impurity content, together with the base precursor composition. Overall, optimising the slag/metakaolin ratio and limestone type enables targeted control over both the fresh-state and early-age evolution of alkali-activated pastes, which is relevant for efficient processing and long-term performance in practical applications.

Acknowledgements

This work was supported by the Czech Science Foundation (GAČR) under project no. 23-05082S.

References

[1] A. M. Rashad. Effect of limestone powder on the properties of alkali-activated materials – A critical overview. *Construction and Building Materials* **356**:129188, 2022. https://doi.org/10.1016/j.conbuildmat.2022.129188

[2] X. Zhu, X. Kang, J. Deng, et al. Chemical and physical effects of high-volume limestone powder on sodium

silicate-activated slag cement (AASC). *Construction and Building Materials* **292**:123257, 2021. https://doi.org/10.1016/j.conbuildmat.2021.123257

[3] X. Gao, Q. L. Yu, H. J. H. Brouwers. Properties of alkali activated slag-fly ash blends with limestone addition. *Cement and Concrete Composites* **59**(1):119–128, 2015. https://doi.org/10.1016/j.cemconcomp.2015.01.007

[4] P. Perez-Cortes, J. I. Escalante-Garcia. Design and optimization of alkaline binders of limestone-metakaolin – A comparison of strength, microstructure and sustainability with portland cement and geopolymers. *Journal of Cleaner Production* **273**:123118, 2020. https://doi.org/10.1016/j.jclepro.2020.123118

[5] J. Qian, M. Song. Study on influence of limestone powder on the fresh and hardened properties of early age metakaolin based geopolymer. In K. Scrivener, A. Favier (eds.), *Calcined Clays for Sustainable Concrete*, vol. 10, pp. 253–259. Springer Netherlands, Dordrecht, 2015. https://doi.org/10.1007/978-94-017-9939-3_31

[6] C. K. Yip, J. L. Provis, G. C. Lukey, J. S. J. van Deventer. Carbonate mineral addition to metakaolin-based geopolymers. *Cement and Concrete Composites* **30**(10):979–985, 2008. https://doi.org/10.1016/j.cemconcomp.2008.07.004

[7] C. Lin Chan, M. Zhang. Effect of limestone on engineering properties of alkali-activated concrete: A review. *Construction and Building Materials* **362**:129709, 2023. https://doi.org/10.1016/j.conbuildmat.2022.129709

[8] B. Felekoğlu, K. Tosun, B. Baradan, et al. The effect of fly ash and limestone fillers on the viscosity and compressive strength of self-compacting repair mortars. *Cement and Concrete Research* **36**(9):1719–1726, 2006. https://doi.org/10.1016/j.cemconres.2006.04.002

[9] N. R. Rakhimova, R. Z. Rakhimov, N. I. Naumkina, et al. Influence of limestone content, fineness, and composition on the properties and microstructure of alkali-activated slag cement. *Cement and Concrete Composites* **72**:268–274, 2016. https://doi.org/10.1016/j.cemconcomp.2016.06.015

[10] J. Xiang, L. Liu, X. Cui, et al. Effect of limestone on rheological, shrinkage and mechanical properties of alkali – Activated slag/fly ash grouting materials. *Construction and Building Materials* **191**:1285–1292, 2018. https://doi.org/10.1016/j.conbuildmat.2018.09.209

[11] X. Dai, S. Aydin, M. Y. Yardimci, et al. Rheology, early-age hydration and microstructure of alkali-activated GGBFS-fly ash-limestone mixtures. *Cement and Concrete Composites* **124**:104244, 2021. https://doi.org/10.1016/j.cemconcomp.2021.104244

[12] H. Mehdizadeh, E. Najafi Kani. Rheology and apparent activation energy of alkali activated phosphorous slag. *Construction and Building Materials* **171**:197–204, 2018. https://doi.org/10.1016/j.conbuildmat.2018.03.130

[13] V. Bilek Jr, M. Pazour. Structural build-up and breakdown of sodium hydroxide-activated slag paste assessed using oscillatory rheology. *Journal of Physics: Conference Series* **2341**(1):012001, 2022. https://doi.org/10.1088/1742-6596/2341/1/012001

[14] D. Jiao, R. De Schryver, C. Shi, G. De Schutter. Thixotropic structural build-up of cement-based materials: A state-of-the-art review. *Cement and Concrete Composites* **122**:104152, 2021. https://doi.org/10.1016/j.cemconcomp.2021.104152

[15] A. M. Mostafa, A. Yahia. New approach to assess build-up of cement-based suspensions. *Cement and Concrete Research* **85**:174–182, 2016. https://doi.org/10.1016/j.cemconres.2016.03.005

[16] X. Dai, S. Aydin, M. Y. Yardimci, G. De Schutter. Rheology and structural build-up of sodium silicate- and sodium hydroxide-activated GGBFS mixtures. *Cement and Concrete Composites* **131**:104570, 2022. https://doi.org/10.1016/j.cemconcomp.2022.104570

[17] D. Kubátová, I. Khongová, M. Krejčí Kotlánová, et al. The use of limestone sludge for the geopolymer preparation. *IOP Conference Series: Materials Science and Engineering* **1205**(1):012002, 2021. https://doi.org/10.1088/1757-899X/1205/1/012002

[18] B. Panda, C. Unluer, M. J. Tan. Investigation of the rheology and strength of geopolymer mixtures for extrusion-based 3D printing. *Cement and Concrete Composites* **94**:307–314, 2018. https://doi.org/10.1016/j.cemconcomp.2018.10.002

[19] M. Stieger. The rheology handbook – For users of rotational and oscillatory rheometers. *Applied Rheology* **12**(5):232–232, 2002. https://doi.org/doi:10.1515/arh-2002-0029

[20] B. Panda, G. B. Singh, C. Unluer, M. J. Tan. Synthesis and characterization of one-part geopolymers for extrusion based 3D concrete printing. *Journal of Cleaner Production* **220**:610–619, 2019. https://doi.org/10.1016/j.jclepro.2019.02.185

[21] P. Rovnaník, P. Rovnaníková, M. Vyšvařil, et al. Rheological properties and microstructure of binary waste red brick powder/metakaolin geopolymer. *Construction and Building Materials* **188**:924–933, 2018. https://doi.org/10.1016/j.conbuildmat.2018.08.150

[22] S. A. Bernal, J. L. Provis, V. Rose, R. Mejia De Gutierrez. Evolution of binder structure in sodium silicate-activated slag-metakaolin blends. *Cement and Concrete Composites* **33**(1):46–54, 2011. https://doi.org/10.1016/j.cemconcomp.2010.09.004

[23] M. Palacios, S. Gismera, M. M. Alonso, et al. Early reactivity of sodium silicate-activated slag pastes and its impact on rheological properties. *Cement and Concrete Research* **140**:106302, 2021. https://doi.org/10.1016/j.cemconres.2020.106302

[24] Y. Liu, B. Dong, Y. Zhang, et al. Limestone powder-based alkali-activated materials: Influence of activator type. *Powder Technology* **434**:119334, 2024. https://doi.org/10.1016/j.powtec.2023.119334

[25] F. J. Huertas, L. Chou, R. Wollast. Mechanism of kaolinite dissolution at room temperature and pressure Part II: Kinetic study. *Geochimica et Cosmochimica Acta* **63**(19–20):3261–3275, 1999. https://doi.org/10.1016/S0016-7037(99)00249-5

[26] R. Mohamed, R. Abd Razak, M. M. A. B. Abdullah, et al. Heat evolution of alkali-activated materials: A review on influence factors. *Construction and Building Materials* **314**:125651, 2022. https://doi.org/10.1016/j.conbuildmat.2021.125651

[27] U. De Filippis, E. Prud'homme, S. Meille. Raw earth stabilised by alkaline activation of slag: Effect of clay on slag hydration. *Materialia* **36**:102143, 2024. https://doi.org/10.1016/j.mtla.2024.102143

[28] A. Chaipanich, K. Wianglor, M. Piyaworapaiboon, S. Sinthupinyo. Thermogravimetric analysis and microstructure of alkali-activated metakaolin cement pastes. *Journal of Thermal Analysis and Calorimetry* **138**(3):1965–1970, 2019. https://doi.org/10.1007/s10973-019-08592-z

[29] A. Cwirzen, J. L. Provis, V. Penttala, K. Habermehl-Cwirzen. The effect of limestone on sodium hydroxide-activated metakaolin-based geopolymers. *Construction and Building Materials* **66**:53–62, 2014. https://doi.org/10.1016/j.conbuildmat.2014.05.022